Microstructure, phase transition, and electrical properties of $(K_{0.5}Na_{0.5})_{1-x}Li_x(Nb_{1-y}Ta_y)O_3$ lead-free piezoelectric ceramics

Dunmin Lin[a)]
Department of Applied Physics and Materials Research Centre, The Hong Kong Polytechnic University, Kowloon, Hong Kong, China and Department of Materials Science, Sichuan University, Chengdu 610064, China

K. W. Kwok and H. L. W. Chan
Department of Applied Physics and Materials Research Centre, The Hong Kong Polytechnic University, Kowloon, Hong Kong, China

(Received 23 January 2007; accepted 17 June 2007; published online 3 August 2007)

Lead-free ceramics $(K_{0.5}Na_{0.5})_{1-x}Li_x(Nb_{1-y}Ta_y)O_3$ have been prepared by an ordinary sintering technique. Our results reveal that Li^+ and Ta^{5+} diffuse into the $K_{0.5}Na_{0.5}NbO_3$ lattices to form a solid solution with a perovskite structure. The substitution of Li^+ induces an increase in the Curie temperature (T_C) and a decrease in the ferroelectric tetragonal–ferroelectric orthorhombic phase transition temperature ($T_{O\text{-}T}$). On the other hand, both T_C and $T_{O\text{-}T}$ decrease after the substitution of Ta^{5+}. A coexistence of the orthorhombic and tetragonal phases is formed at $0.03<x<0.06$ and $0.10<y<0.25$ near room temperature, leading to significant enhancements of the piezoelectric properties. For the ceramic with $x=0.04$ and $y=0.225$, the piezoelectric properties become optimum, giving a piezoelectric coefficient $d_{33}=208$ pC/N, electromechanical coupling factors $k_P=48\%$ and $k_t=49\%$, remanent polarization $P_r=14.2$ μC/cm^2, coercive field $E_c=1.21$ kV/mm, and Curie temperature $T_C=320$ °C. © *2007 American Institute of Physics*. [DOI: 10.1063/1.2761852]

I. INTRODUCTION

Lead zirconate titanate (abbreviated as PZT) and PZT-based ceramics have been widely used in electronic and microelectronic devices because of their excellent piezoelectric and electrical properties. However, because of the toxicity of lead oxide, the use of these ceramics has caused serious environmental problems. Therefore, there is a great need to develop lead-free piezoelectric ceramics with good piezoelectric properties for replacing the lead-containing ceramics in various applications.

A number of lead-free piezoelectric ceramics such as $BaTiO_3$-based ceramics,[1] $Bi_{0.5}Na_{0.5}TiO_3$-based materials,[2–6] tungsten bronze-type materials,[7] Bi-layered structure materials,[8–10] and alkaline niobate-based materials[11–27] have been extensively studied. Among them, $K_{0.5}Na_{0.5}NbO_3$ (abbreviated as KNN) is one of the most promising candidates for lead-free piezoelectric ceramics. It has a high Curie temperature (about 420 °C), good ferroelectric properties ($P_r=33$ μC/cm^2), and large electromechanical coupling factors. However, it is very difficult to obtain dense and well-sintered KNN ceramics using an ordinary sintering process because of the volatility of alkaline elements at high temperatures. For a well-sintered KNN ceramic (e.g., prepared by a hot-pressing technique), it possesses good piezoelectric properties ($d_{33}=160$ pC/N, $k_p=45\%$) and high density ($\rho=4.46$ g/cm^3).[12] However, there is severe degradation in piezoelectric properties ($d_{33}=80$ pC/N, $k_p=36\%$) and density ($\rho=4.25$ g/cm^3) for air-fired KNN ceramics.[11,14] A number of studies have been carried out to improve the properties of KNN ceramics; these include the formation of solid solutions of KNN with other ferroelectrics or nonferroelectrics, e.g., KNN–$LiNbO_3$,[15] KNN–$BaTiO_3$,[18,27] KNN–$SrTiO_3$,[16,17] KNN–$Li(Nb,Ta,Sb)O_3$,[24] KNN–$LiSbO_3$,[26] and the use of sintering aids, e.g., $K_{5.4}Cu_{1.3}Ta_{10}O_{29}$.[20,21] Recently, KNN ceramics comodified with Li and Ta have been studied, and good piezoelectric properties have been reported for several compositions, e.g., $(K_{0.5}Na_{0.5})_{0.96}Li_{0.04}(Nb_{0.90}Ta_{0.10})O_3$ and $(K_{0.5}Na_{0.5})_{0.97}Li_{0.03}(Nb_{0.80}Ta_{0.20})O_3$.[19,24,25] In the present work, KNN ceramics comodified with Li and Ta were prepared by a conventional solid-state sintering process, and their microstructures, phase transformations, and electrical properties (dielectric, ferroelectric, and piezoelectric) were studied systematically.

II. EXPERIMENT

$(K_{0.5}Na_{0.5})_{1-x}Li_x(Nb_{1-y}Ta_y)O_3$ (abbreviated as KNLNT-x/y) ceramics were prepared by a conventional ceramic fabrication technique using analytical-grade metal oxides or carbonate powders: K_2CO_3 (99.9%), Na_2CO_3 (99.8%), Li_2CO_3 (99%), Ta_2O_5 (99%), and Nb_2O_5 (99.95%). The powders in the stoichiometric ratio of the compositions were mixed thoroughly in ethanol using zirconia balls for 8 h, and then dried and calcined at 880 °C for 6 h. After the calcination, the mixture was ball milled again and mixed thoroughly with a polyvinyl alchohol (PVA) binder solution, and then pressed into disk samples with a diameter of 15 mm and a thickness of 0.8 mm. The disk samples were finally sintered at 1090–1190 °C for 4 h in air. Silver electrodes were fired on the top and bottom surfaces of the samples. The ceramics were poled under a dc field of 4–5 kV/mm at 180 °C in a silicone oil bath for 30 min.

a)Electronic mail: ddmd222@yahoo.com.cn

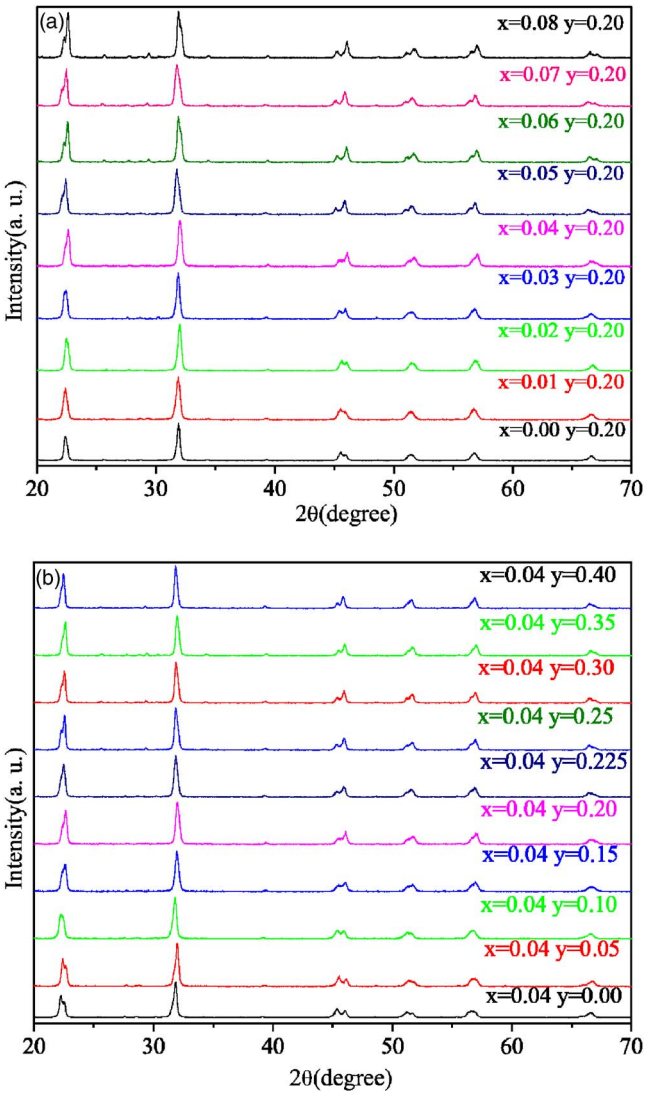

FIG. 1. (Color online) X-ray diffraction patterns of (a) KNLNT-x/0.20 ceramics and (b) KNLNT-0.04/y ceramics.

The crystalline structure of the sintered samples was examined using x-ray diffraction (XRD) analysis with Cu $K\alpha$ radiation (Bruker D8 advance). The microstructure was observed using a scanning electron microscopy (Leica Stereoscan 440). The bulk density ρ was measured by the Archimedes' method. The dielectric constant ε and loss tan δ at 1, 10, and 100 kHz were measured as a function of temperature using an impedance analyzer (HP 4192A). A conventional Sawyer-Tower circuit was used to measure the polarization hysteresis (P-E) loop at 100 Hz. The electromechanical coupling factors k_p and k_t were determined by the resonance method according to Ref. 36 using an impedance analyzer (HP 4294A). The piezoelectric coefficient d_{33} was measured using a piezo-d_{33} meter (ZJ-3A, China).

III. RESULTS AND DISCUSSION

The XRD patterns of the KNLNT-x/0.20 and KLNT-0.04/y ceramics are shown in Fig. 1. As shown in Fig. 1(a), the KNLNT-x/0.20 ceramics, with $x \leqslant 0.05$, possess a pure perovskite structure. At higher concentrations of Li^+, a small amount of secondary phase $K_3Li_2Nb_5O_{15}$ with a tetragonal tungsten bronze structure is formed. It can be also seen that at $x \leqslant 0.02$, the perovskite structure is of the pure orthorhombic phase. As x increases, a tetragonal phase appears, and the structure becomes the pure tetragonal phase at $x \geqslant 0.06$ [Fig. 1(a)]. Similar results are also observed for the KNLNT-0.04/y ceramics [Fig. 1(b)]. At $y < 0.25$, the KNLNT-0.04/y ceramics possess a pure perovskite structure, and a small amount of secondary phase $K_3Li_2Ta_5O_{15}$ with a tetragonal tungsten bronze structure is formed at higher concentrations of Ta^{5+}. The perovskite structure is of the pure orthorhombic phase at $y \leqslant 0.10$ and becomes the pure tetragonal phase at $y \geqslant 0.25$.

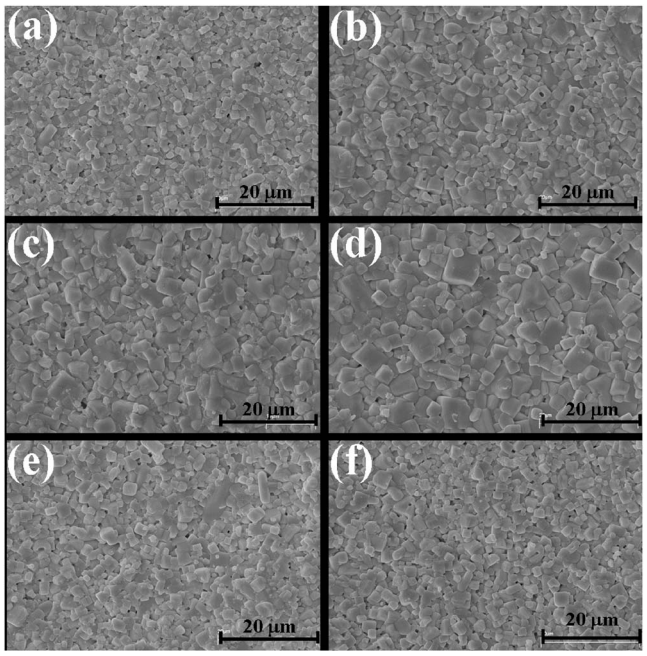

FIG. 2. SEM micrographs of the KNLNT-x/y ceramics: (a) x=0.01, y=0.20, sintered at 1150 °C for 4 h; (b) x=0.05, y=0.20, sintered at 1130 °C for 4 h; (c) x=0.08, y=0.20, sintered at 1120 °C for 4 h; (d) x=0.04, y=0.00, sintered at 1090 °C for 4 h; (e) x=0.04, y=0.225, sintered at 1150 °C for 4 h; and (f) x=0.04, y=0.40, sintered at 1190 °C for 4 h.

On the basis of these results, it can be concluded that Li^+ and Ta^{5+} have diffused into the KNN lattices, with Li^+ entering the $(Na_{0.5}K_{0.5})^+$ sites and Ta^{5+} occupying the Nb^{5+} sites, to form a solid solution. The solubility limit for Li^+ into the A sites of the KNLNT-x/0.20 ceramics is 0.05, while the limit for Ta^+ into the B sites of the KNLNT-0.04/y ceramics is 0.25. Exceeding these limits, secondary phases are formed. It is also suggested that the orthorhombic and tetragonal phases coexist in the KNLNT-x/y ceramics with $0.03 < x < 0.06$ and $0.10 < y < 0.25$ at room temperature.

The scanning electron microscopy (SEM) micrographs of the KNLNT-x/0.20 ceramics are shown in Figs. 2(a)–2(c). For the ceramic with x=0.01, the grains are small, having a diameter ranging from 15 to 2.0 μm. A small amount of pores is also observed in the ceramic [Fig. 2(a)]. As x increases, the grains become larger and the ceramics become denser [Fig. 2(b)]. For the ceramic with x=0.08, the grains are more uniform and have the largest diameter [about 3.5–4.0 μm, Fig. 2(c)]. Unlike Li^+, Ta^{5+} has adverse effects

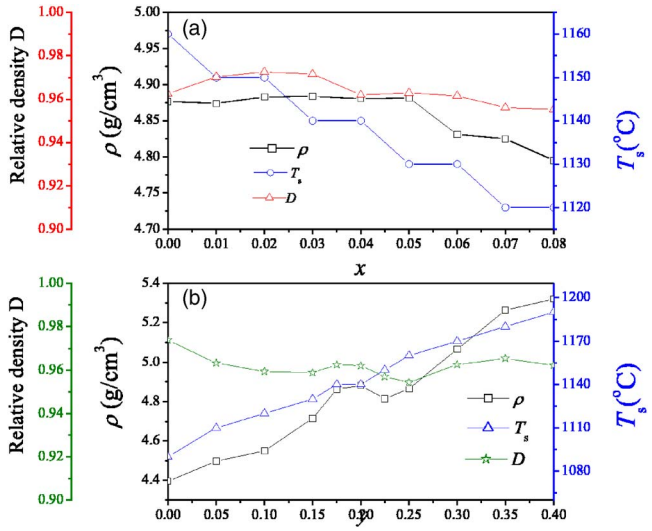

FIG. 3. (Color online) Variations of the density ρ, relative density, and optimum sintering temperatures T_s for (a) KNLNT-x/0.20 ceramics and (b) KNLNT-0.04/y ceramics.

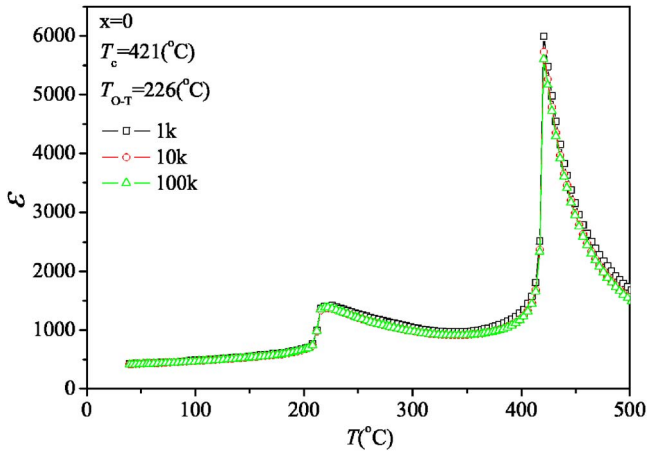

FIG. 4. (Color online) Dielectric constant ε of the KNLNT-0.00/0.00 ceramic as a function of temperature.

on the sintering of the KNLNT-x/y ceramics [Figs. 2(d)–2(f)]. As shown in Fig. 2(d), dense KNLNT-0.04/0.00 ceramics (i.e., Ta-free) can be obtained at a low sintering temperature of 1090 °C. The grains are large, having a diameter of about 4–4.5 μm. However, after the addition of Ta^{5+}, the (optimum) sintering temperature increases, the grains become smaller, and a small amount of pores is even observed [Figs. 2(e) and 2(f)].

The bulk density ρ, relative density D (to the theoretical value), and optimum sintering temperature T_s for the KNLNT-x/0.20 ceramics are shown in Fig. 3(a), while those for the KNLNT-0.04/y ceramics are shown in Fig. 3(b). For each composition, the ceramics were sintered at different temperatures and their density was measured. The optimum sintering temperature was determined as the sintering temperature by which the ceramic had the largest density. As shown in Fig. 3(a), the optimum sintering temperature for the KNLNT-x/0.20 ceramics decreases linearly with increasing x (i.e., the concentration of Li^+). The observed ρ remains almost unchanged ($\sim$4.88 g/cm^3) at $x \leqslant 0.05$ and then decreases slightly to 4.80 g/cm^3 as x increases to 0.08. The decrease in ρ should be due to the small amount of the secondary phase $K_3Li_2Nb_5O_{15}$, which has a lower density (theoretical density $\sim$4.376 g/cm^3). The relative densities of all the samples are higher than 95%, indicating that the ceramics are well sintered. On the basis of these results and the SEM observations [Figs. 2(a)–2(c)], it is clearly seen that the addition of Li^+ improves the sintering performance of the KNN-based ceramics significantly: the sintering temperature is decreased and the densification is enhanced. This may be attributed to the low melting temperature of Li compounds, which promotes the formation of a liquid phase during sintering.

Unlike the KNLNT-x/0.20 ceramics, the optimum sintering temperature for the KNLNT-0.40/y ceramics increases at a rate of about 10 °C/0.05 mol of Ta^{5+} [Fig. 3(b)]. This may be caused by the formation of $KTaO_3$, which has a high melting temperature (1370 °C) (Ref. 20) and hence increases the temperature for forming the solid solutions. However, in spite of the higher sintering temperature, the densification of the ceramics is not good [Figs. 2(e) and 2(f)]. The increase in ρ for the ceramics should be attributed to the higher atomic weight of Ta as compared to Nb [Fig. 3(b)].

Figure 4 shows the temperature dependence of the dielectric constant ε for a pure KNN ceramic. Two transition peaks are observed: one is associated with the paraelectric cubic–ferroelectric tetragonal phase transition at 421 °C (T_C), and the other is the ferroelectric tetragonal–ferroelectric orthorhombic phase transition at 226 °C ($T_{O\text{-}T}$). After the modifications with Li^+ and Ta^{5+}, the KNLNT-x/y ceramics exhibit similar temperature dependences of ε, but with different T_C and $T_{O\text{-}T}$. Figure 5 shows, as examples, the temperature dependences of ε for the KNLNT-0.00/0.20, KNLNT-0.06/0.20, KNLNT-0.04/0.00, and KNLNT-0.04/0.35 ceramics, while the variations of T_C and $T_{O\text{-}T}$ with the concentrations of Li^+ (x) and Ta^{5+} (y) are summarized in Fig. 6.

As shown in Fig. 6(a) for the KNLNT-x/0.20 ceramics, the observed T_C increases linearly from 309 to 355 °C as x increases from 0.00 to 0.06, while $T_{O\text{-}T}$ decreases from 159 to 9 °C at a rate of 20 °C/0.01 mol of Li^+. At higher concentrations of Li^+, T_C remains almost unchanged, while the decrease in $T_{O\text{-}T}$ becomes slower. This may be due to the formation of the secondary phase $K_3Li_2Nb_5O_{15}$. Unlike Li^+, the modification with Ta^{5+} induces a decrease in both T_C and $T_{O\text{-}T}$ [Fig. 6(b)]. T_C decreases linearly at a rate of 30 °C/0.05 mol of Ta^{5+}, while $T_{O\text{-}T}$ decreases from 159 to −50 °C as y increases from 0.00 to 0.40. It can also be seen that the observed $T_{O\text{-}T}$ for the ceramics with x in the range of 0.03 to 0.06 and y in the range of 0.10 to 0.25 are close to room temperature, suggesting that the orthorhombic and tetragonal phases coexist in the ceramics near room temperature. This is consistent with the results of x-ray diffraction (Fig. 1).

Li^+ and Ta^{5+} have different effects on the paraelectric cubic–ferroelectric tetragonal phase transition of the KNLNT-x/y ceramics. KNN is a normal ferroelectric, thus exhibiting a sharp transition peak in the plot of ε versus temperature, as shown in Fig. 4. A substitution of 4 mol %

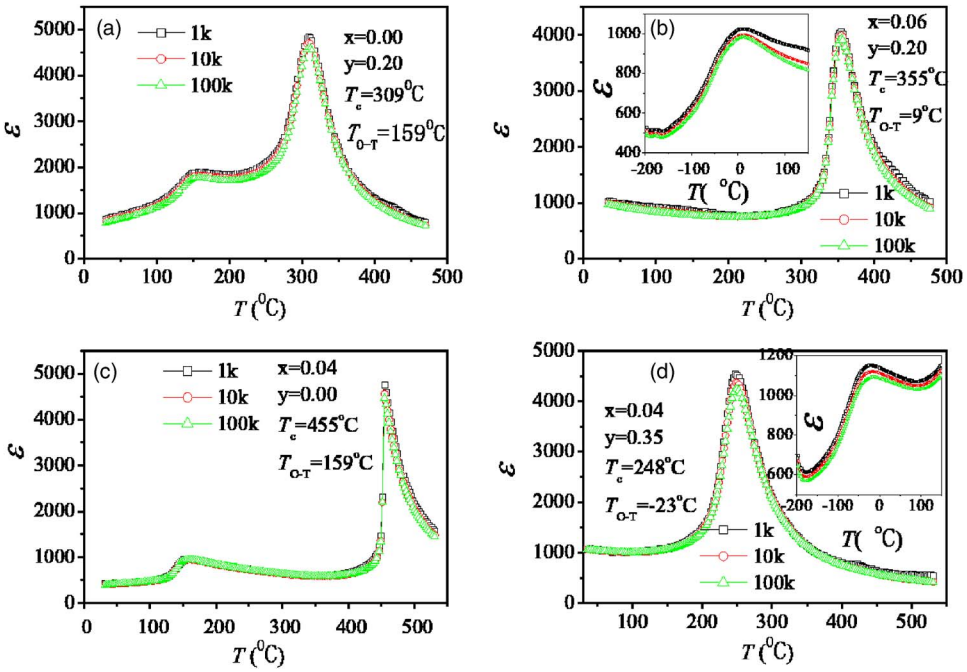

FIG. 5. (Color online) Dielectric constant ε of the KNLNT-x/y ceramics as a function of temperature: (a) $x=0.00$, $y=0.20$; (b) $x=0.06$, $y=0.20$; (c) $x=0.04$, $y=0.00$; and (d) $x=0.04$, $y=0.35$.

Li^+ for $(Na_{0.5}K_{0.5})^+$ does not lead to significant changes in the transition [Fig. 5(c)]. On the other hand, a substitution of 20 mol % Ta^{5+} for Nb^{5+} leads to a broadening of the transition peak, implying a relaxor-type phase transition [Fig. 5(a)]. A diffuse phase transition has been observed in many ABO_3-type perovskites and Bi-layered structure compounds, e.g., $Ba_{0.5}Na_{0.5}TiO_3$-based ceramics,[6,28] $K_{0.5}La_{0.5}Bi_2Nb_2O_9$,[10] $Bi_{0.5}K_{0.5}TiO_3$,[29] Na-modified $Pb_{0.92}(La_{(1-z}Na_z)_{0.08}(Zr_{0.60}Ti_{0.40})_{(0.98+0.4z)}O_3$ (PLZT),[30] $Pb(Sc_{0.5}Ta_{0.5})O_3$,[31] $Pb(Mg_{1/3}Nb_{2/3})O_3$,[32] KNN–$SrTiO_3$.[16] For those compounds, either A sites or B sites are occupied by more than two cations. The diffuseness of the phase transition can be determined from the modified Curie-Weiss law $1/\varepsilon-1/\varepsilon_m=C^{-1}(T-T_m)^{\gamma}$,[32] where ε_m is the maximum value of dielectric constant at the phase transition temperature T_m, γ is the degree of diffuseness, and C is the Curie-like constant. γ can have a value ranging from 1 for a normal ferroelectric to 2 for an ideal relaxor ferroelectric.

Based on the temperature plots of ε at 100 kHz, the graphs of $\log(1/\varepsilon-1/\varepsilon_m)$ vs $\log(T-T_m)$ for the KNLNT-x/y ceramics were plotted, giving the results shown in Fig. 7. All the samples exhibit a linear relationship. By least-squares-

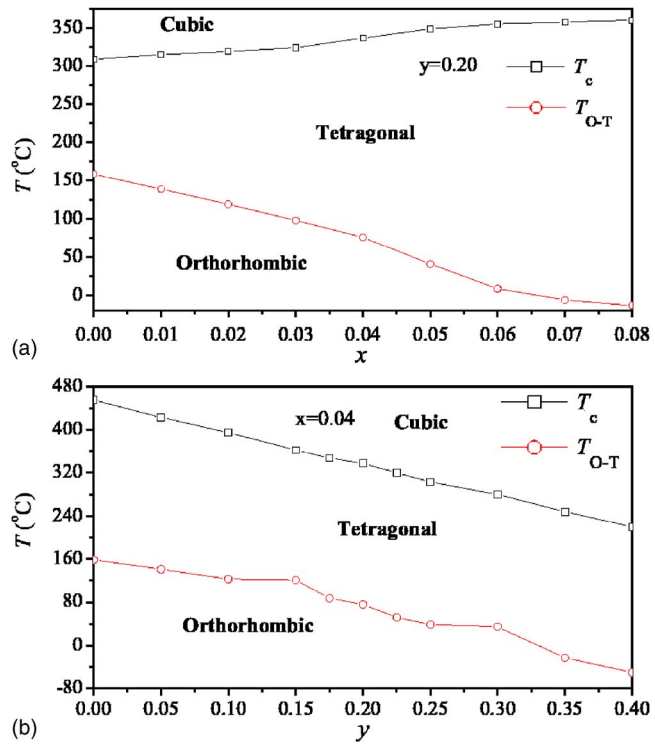

FIG. 6. (Color online) Phase diagrams of (a) KNLNT-$x/0.20$ ceramics and (b) KNLNT-$0.04/y$ ceramics.

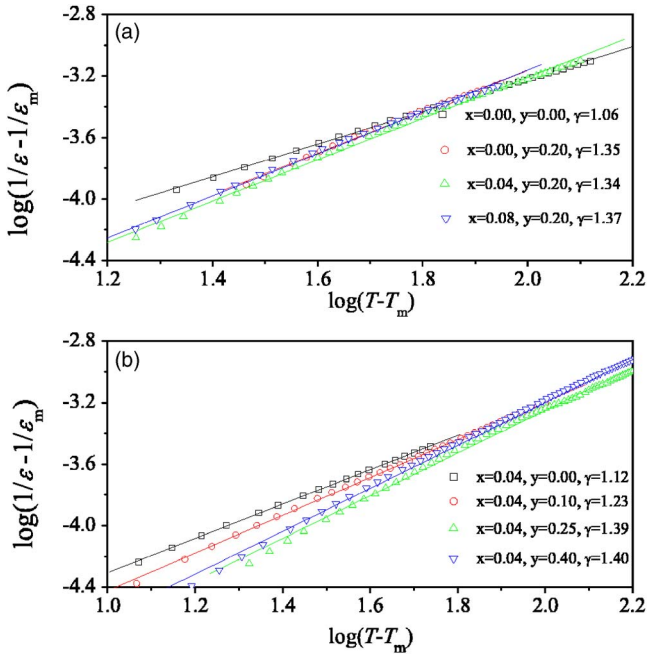

FIG. 7. (Color online) Plot of $\log(1/\varepsilon-1/\varepsilon_m)$ vs $\log(T-T_m)$ for the KNLNT-x/y ceramics. The symbols denote experimental data, while the solid lines denote the least-squares fitting line to the modified Curie-Weiss law.

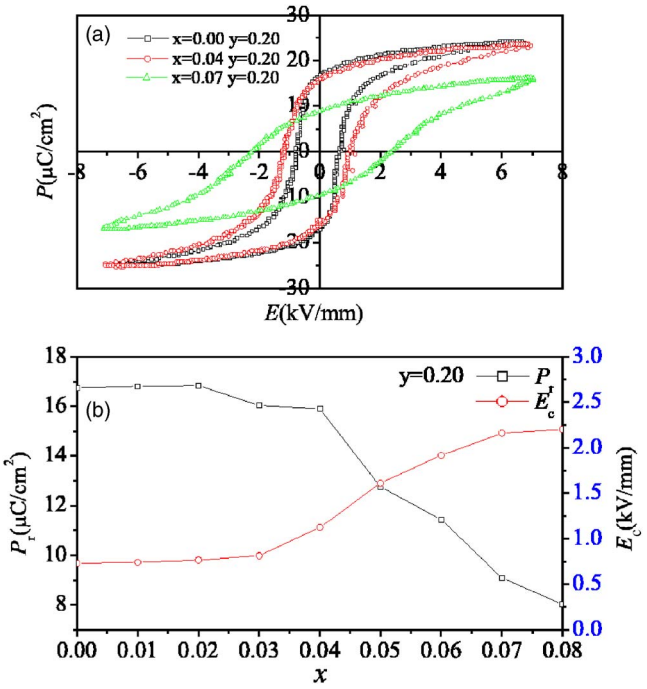

FIG. 8. (Color online) (a) *P-E* hysteresis loops of the KNLNT-x/0.20 ceramics with different x; (b) variations of the remanent polarization P_r and coercive field E_c with x for the KNLNT-x/0.20 ceramics.

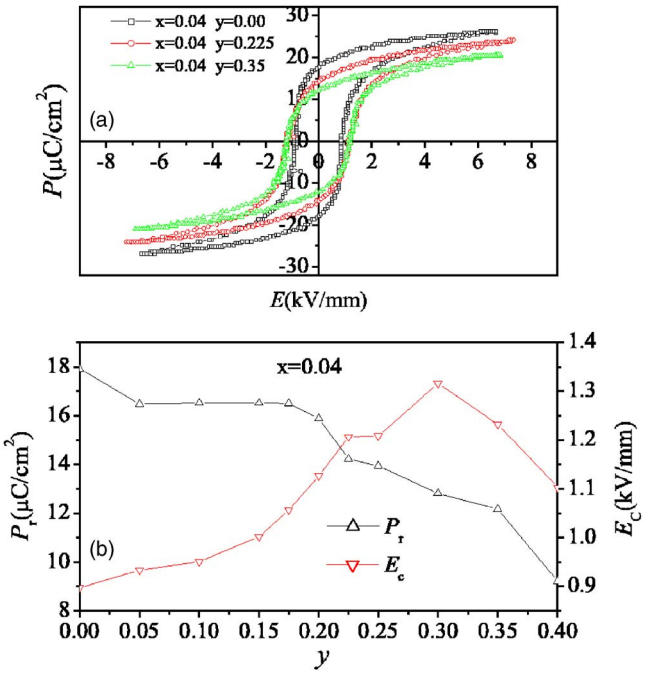

FIG. 9. (Color online) (a) *P-E* hysteresis loops of the KNLNT-0.04/y ceramics with different y; (b) variations of the remanent polarization P_r and coercive field E_c with y for the KNLNT-0.04/y ceramics.

fitting the experimental data to the modified Curie-Weiss law, γ was determined. The calculated γ for the KNLNT-0.00/0.00 (i.e., pure KNN) ceramic is 1.06, revealing its normal ferroelectric characteristics [Fig. 7(a)]. After the substitution of 4 mol % Li^+, γ increases slightly to 1.12, suggesting that the substitution does not induce significant changes in the phase transition and that the KNLNT-0.04/0.00 ceramic is still a normal ferroelectric [Fig. 7(b)]. Similar results are also observed for the KNLNT-x/0.20 ceramics. As x increases, γ remains almost unchanged at a value of about 1.35 [Fig. 7(a)]. The large γ value results from the substitution of Ta^{5+}. As shown in Fig. 7(b), γ increases with increasing y for the KNLNT-0.04/y ceramics. This suggests that the substitution of Ta^{5+} makes the KNLNT-x/y ceramics become more relaxor, thus exhibiting a broadened transition peak, as shown in Figs. 5(c) and 5(d).

It has been known that for the A-site complex $(A_1A_2)BO_3$ or B-site complex $A(B_1B_2)O_3$ perovskite ferroelectrics, a large difference in ionic radii of the A-site cations or B-site cations is favorable for the formation of an ordered structure.[6,32] As Li^+ is smaller than Na^+ and K^+ (0.68 Å vs 0.97 and 1.38 Å), the substitution of Li^+ for the A sites Na^+ and K^+ in the KNLNT-x/0.00 and KNLNT-x/0.20 ceramics should be favorable for forming an ordered structure; hence, the disordered degree of the ceramics in the A site does not increase considerably. On the other hand, due to the small difference in the ionic radii between Nb^{5+} (0.69 Å) and Ta^{5+} (0.68 Å), the substitution of Ta^{5+} for Nb^{5+} increases the B-site disordered degree and hence the local compositional fluctuation. As a result, the ceramics become more relaxor and exhibit a diffuse phase transition.

All the ceramics (KNLNT-x/0.20 and KNLNT-0.04/y) exhibit a well-saturated *P-E* loop under an electric field of about 7 kV/mm. Figure 8(a) shows, as examples, the *P-E* loops for the KNLNT-x/0.20 ceramics, with x=0.00, 0.04, and 0.07, while the *P-E* loops for the KNLNT-0.04/y ceramics, with y=0.00, 0.225, and 0.35, are shown in Fig. 9(a). The variations of the remanent polarization P_r and coercive field E_c with x and y for the ceramics are shown in Figs. 8(b) and 9(b), respectively. For the KNLNT-x/0.20 ceramics, both P_r and E_c remain almost unchanged at $x \leqslant 0.03$ [Fig. 8(b)]. As x increases from 0.03 to 0.08, P_r starts to decrease linearly from 16.0 to 8.0 $\mu C/cm^2$, while E_c increases from 0.81 to 2.20 kV/mm. As shown in Fig. 9(b) for the KNLNT-0.04/y ceramics, P_r decreases slightly from 17.9 to 16.5 $\mu C/cm^2$ as y increases from 0 to 0.175, and then decreases rapidly with increasing y. E_c increases significantly with increasing y and then decreases, giving a maximum value of 1.32 kV/mm at y=0.30. These clearly show that the substitution of Li^+ and Ta^{5+} has weakened the ferroelectric properties of the KNN-based ceramics.

The variations of the piezoelectric coefficient d_{33}, electromechanical coupling factors k_P and k_t, dielectric constant ε, and loss tan δ with x for the KNLNT-x/0.20 ceramics are shown in Fig. 10, while the variations of those properties with y for the KNLNT-0.04/y ceramics are shown in Fig. 11. For the KNLNT-x/0.20 ceramics, d_{33} increases sharply with increasing x and then decreases, giving a maximum value of 174 pC/N at x=0.04 [Fig. 10(a)]. Similar to d_{33}, k_P, k_t, and ε reach a maximum value of 44%, 46%, and 1146, respectively, at x=0.04. On the other hand, tan δ remains almost unchanged at a value smaller than 4% [Fig. 10(b)]. As shown in Fig. 11, the KNLNT-0.04/y ceramic exhibits similar compositional dependences of d_{33}, k_p, k_t, and ε. All of them reach a maximum value at y=0.225, which are about 208 pC/N,

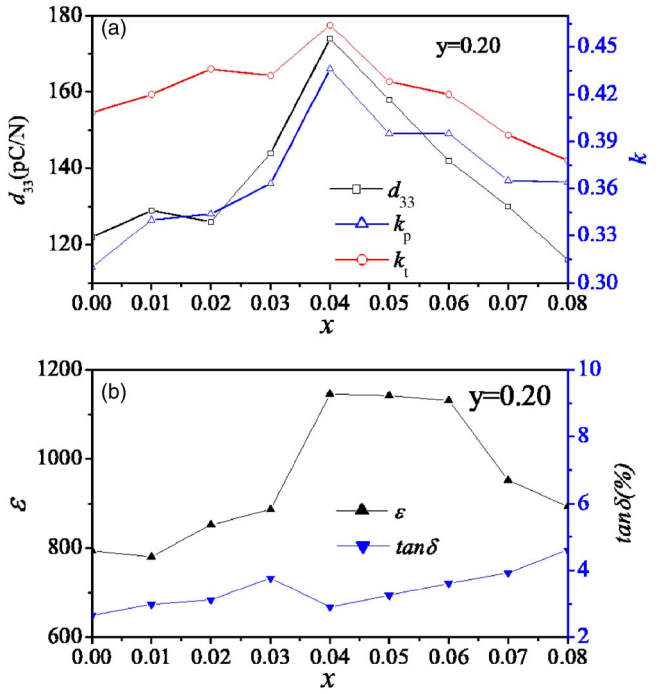

FIG. 10. (Color online) (a) Variations of the piezoelectric coefficient d_{33} and electromechanical coupling factors k_P and k_t with x for the KNLNT-x/0.20 ceramics; (b) variations of the dielectric constant ε and loss tan δ with x for the KNLNT-x/0.20 ceramics.

48%, 49%, and 1146, respectively. tan δ remains at a value smaller than 3% in the range of y from 0 to 0.40 [Fig. 11(b)].

Figure 12 shows the thermal-depoling behavior of the KNLNT-0.04/0.225 ceramic (which has the optimum dielectric and piezoelectric properties). The poled sample was annealed at elevated temperatures for 1 h, and then its d_{33} was

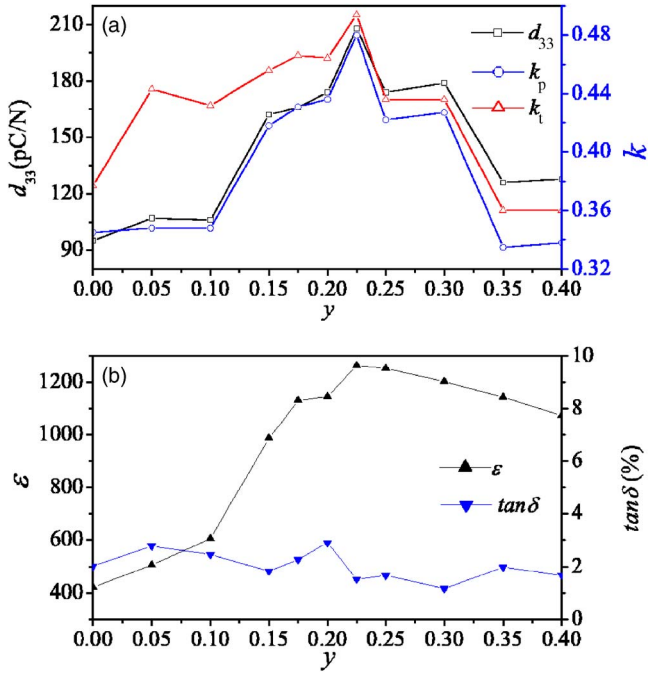

FIG. 11. (Color online) (a) Variations of the piezoelectric coefficient d_{33} and electromechanical coupling factors k_P and k_t with y for the KNLNT-0.04/y ceramics; (b) variations of the dielectric constant ε and loss tan δ with y for the KNLNT-0.04/y ceramics.

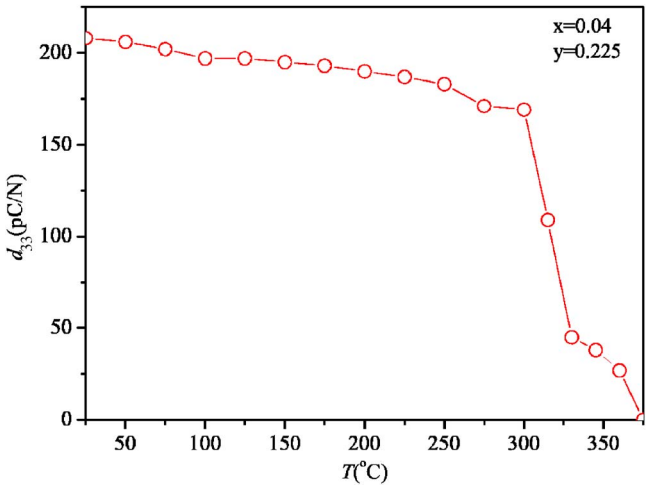

FIG. 12. (Color online) Variation of the piezoelectric coefficient d_{33} with the annealing temperature for the KNLNT-0.04/0.225 ceramic.

reevaluated. As shown in Fig. 12, d_{33} decreases slowly from 208 to 169 pC/N as the annealing temperature increases from 25 to 300 °C, and then decreases rapidly to zero at ~375 °C. The observed T_C for the ceramic from the dielectric measurement is about 320 °C.

It is well known that the morphotropic phase boundary (MPB) plays a very important role in the improvement of piezoelectric properties of perovskite piezoelectric ceramics, such as PZT,[33] $Pb(Mg_{1/3}Nb_{2/3})O_3$–$PbTiO_3$,[34] $Bi_{0.5}Na_{0.5}TiO_3$–$BaTiO_3$,[2] $Bi_{0.5}Na_{0.5}TiO_3$–$Bi_{0.5}K_{0.5}TiO_3$.[5] In general, a MPB is defined as an abrupt structural change for a solid solution with variation in composition.[33–35] The term "morphotropic" means literally "the boundary between two forms."[33–35] Typically, the change is nearly independent of temperature, giving a nearly vertical line in the phase diagram such as those for the PZT, $Pb(Mg_{1/3}Nb_{2/3})O_3$–$PbTiO_3$ (PMN-PT), and $Bi_{0.5}Na_{0.5}TiO_3$-based systems.[2,5,33,34] It is generally believed that the enhancement in piezoelectric properties of the ceramics near the MPB is mainly attributed to the more possible polarization states resulting from the coexistence of the two phases. Unlike PZT and other systems, the phase transitions for the KNLNT-x/y ceramics depend not only on the compositions but also on the temperature (Fig. 6). Although the phase boundary between the orthorhombic and tetragonal phases may not be a MPB, it is believed to be the major origin for the enhancement in piezoelectric properties of the ceramics. Similar to the other systems with MPB, the KNLNT-x/y ceramics with x in the range of 0.03 to 0.06 and y in the range of 0.10 to 0.25 contain both the orthorhombic and tetragonal phases near room temperature (Figs. 1 and 6) and thus more possible polarization states. Therefore, although the ceramic with x =0.04 and y=0.225 does not possess the largest P_r (14.2 μC/cm^2), it exhibits the optimum piezoelectric properties (d_{33}=208 pC/N, k_P=48.0%, and k_t=49.4%). On the other hand, although the KNLNT-0.06/0.20 and KNLNT-0.04/0.25 ceramics may contain both the orthorhombic and tetragonal phases, they contain secondary phase ($K_3Li_2Nb_5O_{15}$ and $K_3Li_2Ta_5O_{15}$, respectively), and hence their piezoelectric properties become poorer (Figs. 1, 8, and 9).

IV. CONCLUSIONS

Lead-free KNLNT-x/y piezoelectric ceramics have been prepared by a conventional ceramic sintering technique, and their microstructures, phase transitions, and electrical properties have been investigated in detail. Our results reveal that Li^+ and Ta^{5+} diffuse into the $K_{0.5}Na_{0.5}NbO_3$ lattices to form a solid solution with a perovskite structure. The solubility limits for Li^+ and Ta^{5+} in the KNLNT-x/y perovskites are 0.05 and 0.25, respectively. The substitution of Li^+ decreases the sintering temperature of the ceramics, assists the densification, increases T_C, and decreases T_{O-T}. Unlike Li^+, the substitution of Ta^{5+} leads to an increase in the sintering temperature and a decrease in both T_C and T_{O-T}. It also makes the ceramics become more relaxor, showing a diffuse phase transition at T_C. The coexistence of the orthorhombic and tetragonal phases is formed in the ceramics with $0.03<x<0.06$ and $0.15<y<0.25$, leading to a significant enhancement of the piezoelectric properties. For the ceramic with $x=0.04$ and $y=0.225$, the piezoelectric properties become optimum, giving $d_{33}=208$ pC/N, $k_P=48\%$, and $k_t=49\%$. Because of the high T_C (320 °C), it also exhibits a good temperature stability.

ACKNOWLEDGMENTS

This work was supported by the Innovation and Technology Fund (ITF GHS/066/04) and the Center for Smart Materials of The Hong Kong Polytechnic University.

[1]Z. Yu, C. Ang, R. Guo, and A. S. Bhalla, J. Appl. Phys. **92**, 1489 (2002).
[2]T. Takenaka, K. Maruyama, and K. Sakata, Jpn. J. Appl. Phys., Part 1 **30**, 2236 (1991).
[3]X. Wang, X. G. Tang, and H. L. W. Chan, Appl. Phys. Lett. **85**, 91 (2004).
[4]D. Lin, D. Xiao, J. Zhu, and P. Yu, Appl. Phys. Lett. **88**, 062901 (2006).
[5]A. Sasaki, T. Chiba, Y. Mamiya, and E. Otsuki, Jpn. J. Appl. Phys., Part 1 **38**, 5564 (1999).
[6]Y. Li, W. Chen, Q. Xu, J. Zhou, X. Gu, and S. Fang, Mater. Chem. Phys. **94**, 328 (2005).
[7]R. Xie, Y. Akimune, K. Matsuo, T. Sugiyama, N. Hirosaki, and T. Sekiya, Appl. Phys. Lett. **80**, 835 (2002).
[8]R. Jain, A. K. S. Chauhan, V. Gupta, and K. Sreenivas, J. Appl. Phys. **97**, 124101 (2005).
[9]W. Li, J. Gu, C. Song, D. Su, and J. Zhu, J. Appl. Phys. **98**, 114104 (2005).
[10]C. Karthik, N. Ravishankar, and K. B. R. Varma, Appl. Phys. Lett. **89**, 042905 (2006).
[11]L. Egerton and D. M. Dillom, J. Am. Ceram. Soc. **42**, 438 (1959).
[12]R. E. Jaeger and L. Egerton, J. Am. Ceram. Soc. **45**, 209 (1962).
[13]R. H. Dungan and R. D. Golding, J. Am. Ceram. Soc. **48**, 601 (1965).
[14]Z. S. Ahn and W. A. Schulze, J. Am. Ceram. Soc. **70**, 18 (1987).
[15]Y. Guo, K. Kakimoto, and H. Ohsato, Appl. Phys. Lett. **85**, 4121 (2004).
[16]Y. Guo, K. Kakimoto, and H. Ohsato, Solid State Commun. **129**, 279 (2004).
[17]R. Wang, R. Xie, K. Hanada, K. Matsusak, H. Bando, and M. Itoh, Phys. Status Solidi A **202**, R57 (2005).
[18]C. W. Ahn, H. C. Song, S. Nahm, S. H. Park, K. Uchino, S. Priya, H. G. Lee, and N. K. Kang, Jpn. J. Appl. Phys., Part 1 **44**, L1361 (2005).
[19]E. Hollenstein, M. Davis, D. Damjanovic, and N. Setter, Appl. Phys. Lett. **87**, 182905 (2005).
[20]M. Matsubara, K. Kikuta, and S. Hirano, J. Appl. Phys. **97**, 114105 (2005).
[21]M. Matsubara, T. Yamaguchi, W. Sakamoto, K. Kikuta, T. Yogo, and S. Hirano, J. Am. Ceram. Soc. **88**, 1190 (2005).
[22]H. Takao, Y. Saito, Y. Aoki, and K. Horibuchi, J. Am. Ceram. Soc. **89**, 1951 (2006).
[23]R. Zuo, J. Rödel, R. Chen, and L. Li, J. Am. Ceram. Soc. **89**, 2010 (2006).
[24]Y. Saito, H. Takao, T. Tani, T. Nonoyama, K. Takatori, T. Homma, T. Nagaya, and M. Nakamur, Nature (London) **432**, 84 (2004).
[25]Y. Guo, K. Kakimoto, and H. Ohsato, Mater. Lett. **59**, 241 (2005).
[26]G. Zang *et al.*, Appl. Phys. Lett. **88**, 212908 (2006).
[27]H. Y. Park, C. W. Ahn, H. C. Song, J. H. Lee, S. Nahm, K. Uchino, H. G. Lee, and H. J. Lee, Appl. Phys. Lett. **89**, 062906 (2006).
[28]S. Saïd and J. P. Mercurio, J. Eur. Ceram. Soc. **21**, 1333 (2001).
[29]Z. F. Li, C. L. Wang, W. L. Zhong, J. C. Li, and M. L. Zhao, J. Appl. Phys. **94**, 2548 (2003).
[30]S. Shannigrahi, P. N. P. Choudary, H. N. Acharya, and T. P. Sinha, J. Phys. D **32**, 1539 (1999).
[31]N. Setter and L. E. Cross, J. Appl. Phys. **51**, 4356 (1980).
[32]K. Uchino, S. Nomura, L. E. Cross, S. J. Tang, and R. E. Newnham, J. Appl. Phys. **51**, 1142 (1980).
[33]B. Noheda, D. E. Cox, G. Shirane, R. Guo, B. Jones, and L. E. Cross, Phys. Rev. B **63**, 014103 (2000).
[34]B. Noheda, D. E. Cox, G. Shirane, J. Gao, and Z. G. Ye, Phys. Rev. B **66**, 054104 (2002).
[35]B. Jaffe, W. R. Cook, and H. Jaffe, *Piezoelectric Ceramics* (Academic Press, London, 1971), pp. 135–183.
[36]IEEE Standard on Piezoelectricity, IEEE Std. 176-1987, New York: The Institute of Electrical and Electronics Engineers, 1987.